Improved Measurement of Preheat in Cryogenic Targets

Introduction

Preheat by fast electrons in cryogenic target implosions is thought to be a crucial parameter in determining target performance, primarily the achieved areal density. To quantitatively relate the achieved areal density to the fuel preheat, the preheat measurement has to be sufficiently reliable and precise. In addition, the validity of the assumptions used in the data analysis and the resulting uncertainty have to be determined. To that end this article presents a reformulated and more consistent analysis of preheat measurements and discusses the sensitivity of the results to the assumptions made in the analysis. The results are applied to both cryogenic and CH targets.

Details of the method of analysis are described in Ref. 1. The preheat is determined from the hard x-ray (HXR) bremsstrahlung radiation; the HXR detector is calibrated by using a CH-coated molybdenum (Mo) solid sphere where the preheat is determined using the Mo K_α line. The resulting calculated curves for both cryogenic and CH targets directly relate the HXR signal to the preheat. The curves are plotted as a function of fast-electron temperature, which is also measured by the HXR detectors.

The main improvement with respect to previous results[1] is the folding of the HXR sensitivity curve[2] into the calculation of emitted radiation. The total bremsstrahlung radiation for a given electron energy is taken from the NIST tables,[3] but the folding also requires the spectrum of the radiation. That spectrum is a function of the photon energy E_p and the electron energy E_e ($E_p < E_e$); the spectrum is usually plotted as a function of $R = E_p/E_e$ but still depends separately on E_e. The folding with detector sensitivity has to be done for each electron energy. Also, because the electron-energy distribution changes due to the transport through the target, the folding is done at each target location. The bremsstrahlung spectra were tabulated in papers by Seltzer *et al.*[4] and Pratt *et al.*,[5] on which the NIST tables are based. *Thus, the calibration of the HXR detector is not a stand-alone number but is intertwined with the radiation spectrum and thus with the electron-energy distribution*. The detector measures only the absorbed radiation, and the derivation of incident radiation is model dependent. The radiation spectrum is calculated from the electron-energy distribution but the latter has to be assumed.

A simplified, generic formulation of bremsstrahlung radiation given by Jackson[6] is often used. Figure 112.12 compares the total radiation emitted by an electron traveling in Mo, calculated using Eq. (15.30) in Ref. 6 and as given by the NIST tables. Jackson's formula is insufficient for precise calculations of preheat.

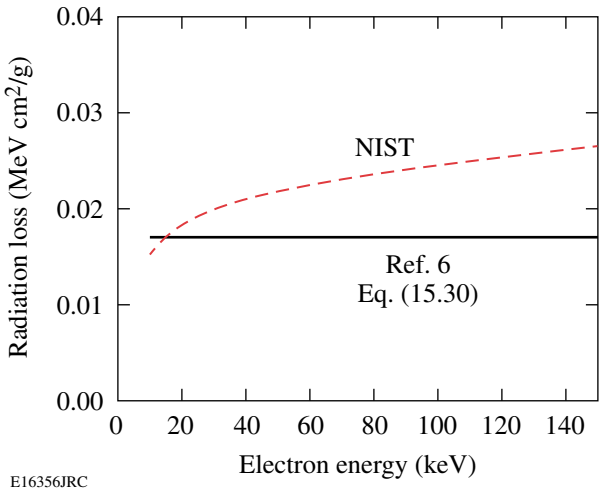

Figure 112.12
Comparison of the total radiation emitted by an electron traveling in Mo, as a function of its energy. The upper curve is given by the NIST tables;[3] the lower curve is calculated by Jackson [Eq. (15.30) in Ref. 6]. Jackson's formula is insufficient for precise calculations of preheat.

Effective Detector Sensitivity

The folding of detector sensitivity described here was done for the three cases of Mo, CH, and cryogenic D_2 (or DT) targets. The relative sensitivity of the HXR detector $S(E_p)$ as a function of photon energy is given in Ref. 2. $S(E_p)$ is the fraction of radiation absorbed in the detector. The fraction of the radiation energy emitted by an electron of energy E_e that is absorbed by the detector is given by

$$S_{\text{eff}}(E_e) = \frac{\int \text{bremss}(E_e, E_p) S(E_p) \mathrm{d}E_p}{\int \text{bremss}(E_e, E_p) \mathrm{d}E_p}, \quad (1)$$

where "bremss" is the bremsstrahlung spectrum (from Refs. 4 and 5). Figure 112.13 shows the calculated S_{eff} for a few materials. As seen, the effective sensitivity depends weakly on the material. The total energy radiated by an electron of energy E_e that is absorbed in the detector is given by

$$E_{\text{abs}}(E_e) = S_{\text{eff}}(E_e) \times \text{NIST}_{\text{bremss}}(E_e), \quad (2)$$

where $\text{NIST}_{\text{bremss}}$ is the total radiation emitted by an electron of energy E_e, per cm traveled, and is given by the NIST tables.[3] In the transport calculations described below, the results of Eq. (2), using curves like those in Fig. 112.13, are summed over the electron-energy distribution $D(E_e)$ at each target location. Summing over the target volume yields the total radiation energy absorbed in the detector for a given energy in the fast electrons. The calibration described below relates the energy absorbed in the detector to the detector reading (in pC). The initial distribution $D(E_e)$ is guessed and is then modified by the transport through the target. Three initial shapes for $D(E_e)$ were tested:

$$\begin{aligned} &\text{(a) exponential:} && D(E_e) = \exp(-E_e/T_e) \\ &\text{(b) Maxwellian:} && D(E_e) = E_e^{1/2} \exp(-E_e/T_e) \\ &\text{(c) truncated:} && D(E_e) = \begin{cases} \exp(-E_e/T_e) \\ 0 \text{ for } E_e > 3T_e \end{cases} \end{aligned} \quad (3)$$

Distributions (b) and (c) can be thought of as two extremes of (a): in (b) the low-energy part of $D(E_e)$ is reduced, whereas in (c) the high-energy part of $D(E_e)$ is reduced. Since low-energy electrons are more efficient in collisions whereas high-energy electrons are more efficient in radiation, the ratio of preheat to radiation, as expected, is found to increase in going from (b) to (a) to (c).

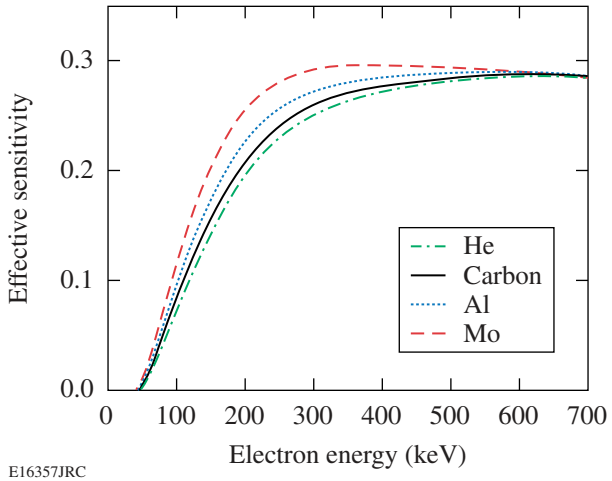

Figure 112.13
Effective sensitivity: the fraction of the radiation emitted by an electron of energy E_e that is absorbed in the detector (HXR2), using Eq. (1). These curves, summed over the assumed electron-energy distribution (for the known temperature), relate the radiation energy absorbed in the detector to the energy in fast electrons.

The Mo Target Calibration Experiment

The preheat energy in any target experiment is determined from the HXR signal. To calibrate the HXR detector in absolute units, we used an ~0.9-mm-diam molybdenum solid sphere, coated with a 20-μm-thick CH layer. The target was irradiated with the 60 OMEGA beams at an intensity of ~1×10^{15} W/cm^2 and a 1-ns square pulse.[1] The preheat was determined from the Mo K_α line and related to the HXR signal. The measured Mo K_α energy was 9.4 mJ (per total solid angle). The HXR2 channel (used to determine the total radiation) measured a signal of 1200 pC, and comparison of channels 2, 3, and 4 yielded a fast-electron temperature of T_e = 65 keV.

A 1-D multi-energy transport code was used to transport fast electrons of varying temperatures for each of the three chosen shapes [Eq. (3)]. The calculations using a stationary target are time integrated over the pulse, as are the measurements of K_α and HXR energies. In a 1-D calculation, only radial trajectories are considered. For the Mo target this is justified because *LILAC* simulations show that at the end of the pulse the quarter-critical density is ~100 μm away from the target surface, a distance much smaller than the target diameter. At the end of the pulse (when most of the fast electrons are generated) the thickness of the unablated CH layer is ~10 μm. Therefore, in the calculations we assumed a cold, 10-μm-thick CH layer. When the calculations were repeated for a 15-μm CH thickness, the resulting calibration was hardly changed. The transport code calculates the slowing down of electrons, the production and transport of K_α energy, and the production of HXR continuum. For the slowing down and the HXR production, the NIST tables are used; for the K_α production a semi-empirical cross section[7] is used. The transport code shows that more than 99% of the HXR comes from the Mo; however, some of the electron energy (~10%) is deposited in the CH and must be subtracted from the total deposited energy. Two ratios are computed: PH/K_α = (preheat energy)/(K_α energy) and

PH/HXR-abs = (preheat energy)/(energy absorbed in HXR2), both as a function of T_e. The K_α energy refers to the energy exiting the target after absorption within the molybdenum. Here, we need only the results for the case of the Mo experiment (T_e = 65 keV), which we quote in Table 112.III. The absorption of the K_α line within the target increases with electron temperature because higher-energy electrons penetrate deeper; for T_e = 65 keV that absorption is only ~30%.

Table 112.III shows the Mo target analysis results for the three electron distributions considered. Row 1 shows the ratio of preheat to emergent K_α energy. For the measured K_α energy of 9.4 mJ, row 2 shows the preheat energy within the molybdenum. Row 3 shows the ratio of preheat energy to HXR energy absorbed in the detector. Dividing row 2 by row 3 yields the total energy absorbed in the HXR2 detector. Finally, dividing the measured HXR2 signal of 1200 pC by row 4 yields detector absolute calibration, namely the signal in HXR2 (in pC) per radiation energy absorbed in HXR2 (in mJ).

As explained above, the ratio PH/HXR-abs increases in going from (b) to (a) to (c) because the relative number of low-energy electrons in the distribution increases. This is also true for the ratio PH/K_α, but here the change is very small (~6%). This can be shown to be due to the differences in the cross sections for producing K_α and bremsstrahlung radiation. The calibration factor is seen to change appreciably with the change in assumed distribution shape. However, as shown below, in calculating preheat in cryogenic or CH targets, the differences between the three distribution shapes become considerably smaller. This is because the ratio PH/HXR in CH or cryogenic targets is also dependent on the distribution shape, and when applying the corresponding calibration factor from Table 112.III, these differences partly cancel out.

Preheat in CH Targets

The ratio of preheat to the HXR2 signal for CH targets was calculated as a function of temperature of the fast electrons, for each of the three electron-distribution shapes of Eq. (3). As in the case of Mo, the NIST tables are used for both the slowing down (collisions) and the bremsstrahlung radiation. The corresponding calibration numbers of Table 112.III were used to convert radiation energy absorbed in the detector to the signal in pC. We assumed that the shape of the electron distribution is the same in the Mo experiment as in CH target experiments. This assumption is reasonable since in both cases (as well as in the cryogenic targets discussed below) the laser interacts with a CH layer. Thus, for each of the three distribution shapes, we used the corresponding calibration factor from Table 112.III. The results for a 10-μm-thick CH target are shown in Fig. 112.14. The variation around the average for all temperatures is ±25%. This represents the range of uncertainties in the preheat determination. To illustrate how the results depend on the target thickness, we show in Fig. 112.15 the ratio for a Maxwellian electron distribution, for three different thicknesses. The ratio of preheat to the HXR2 signal is almost independent of the target thickness. For electrons of a single

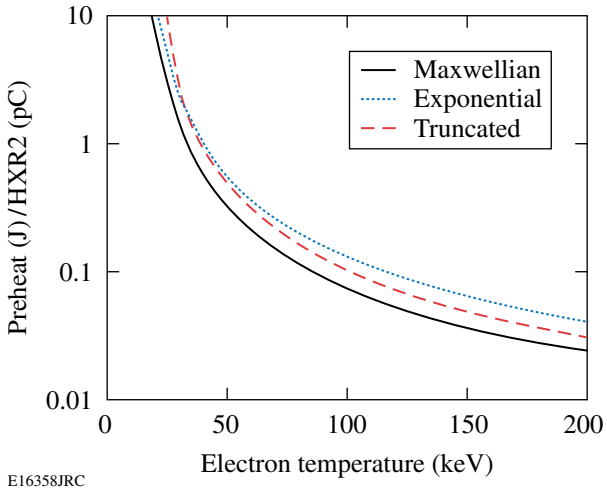

Figure 112.14
The ratio of preheat energy deposited by fast electrons in a 10-μm-thick CH target to the HXR2 reading (pC) for three assumed distributions of electron energies.

Table 112.III: Calculated quantities involved in determining the HXR detector calibration from the Mo experiment, for three electron-energy distribution shapes

	Quantity Calculated	(a) Exponential	(b) Maxwellian	(c) Truncated
1	Preheat/K_α	1058	996	1063
2	Mo preheat	9.945 J	9.36 J	10.0 J
3	Preheat/HXR-abs	1704	1355	2503
4	HXR-abs	5.83 mJ	6.9 mJ	4.0 mJ
5	Calibration (pC/mJ)	205	174	300

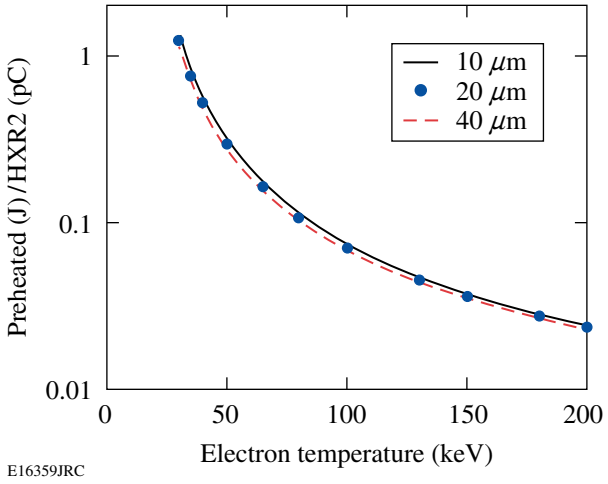

Figure 112.15
Ratio of preheat energy deposited by fast electrons in CH to HXR2 reading (pC) for three thicknesses of the CH target. A Maxwellian distribution of electron energies was assumed.

energy E_e, the ratio increases with thickness (until the thickness exceeds the range corresponding to E_e) because a thicker target yields slower electrons, for which the preheat increases (as ~1/E), whereas the radiation decreases (see Fig. 112.12). However, for the case of continuous distribution of energies, the shift of the distribution to lower energies is equivalent to lowering the distribution, which does not affect the ratio of the two plotted quantities.

Preheat in Cryogenic Targets

To calculate the preheat and x-ray emission from cryogenic targets we use again a 1-D, multi-energy transport code. However, unlike the case of the CH-coated Mo target, the fraction of radiation emitted by the CH shell is not negligible and its calculation requires a multidimensional treatment of the fast-electron transport. This is because when the fast electrons are generated, the quarter-critical surface is far enough from the target to enable many trajectories that miss the cold-fuel shell. Thus, before applying the preheat results derived here, that fraction has to be determined separately. Using the measured radiation that is emitted by the fuel leads to the determination of the preheat within the fuel alone. The deposition of electron energy within the CH shell is irrelevant to the determination of fuel preheat, but it affects the preheat results marginally since it changes the energy distribution of the electrons entering the fuel. As will be shown below, the results are weakly dependent on that distribution. For the calculation of radiation we again use the NIST tables. However, for the collisional transport (preheat) we must use the formula for slowing down in a plasma since the fuel is fully ionized even with no preheat. We use Eq. (1) of Ref. 1:

$$\left(-\mathrm{d}E/\mathrm{d}x\right) = \left(2\pi e^4 N_e/E\right) \ln\left(1.52\, E/\hbar\,\omega_p\right) \qquad (4)$$

in terms of the electron density and the plasma frequency. This equation is essentially identical to Eq. (13.88) given by Jackson in Ref. 6. We used the plasma density profile calculated by *LILAC* at the end of the laser pulse (when most of the $2\omega_p$ electrons were found to be generated); however, the results are shown to be insensitive to this choice.

For transport in un-ionized material, the dependence on electron density of the ratio preheat/radiation cancels out. However, because of the appearance of the plasma frequency in the Coulomb logarithm in Eq. (4), we must consider the density profile of a particular case. We used the plasma density profile calculated by *LILAC* for a typical D_2 cryogenic target shot at an irradiance of 5×10^{14} W/cm^2, at the end of the laser pulse. Figure 112.16 shows curves for the ratio of preheat to energy absorbed in the detector for the three distribution shapes; Fig. 112.17 shows the curves after applying the calibration from Table 112.III. The total relative span of the three curves around an average is ~20%. To test the sensitivity of the results to the density profile, Fig. 112.18 shows the effect of multiplying or dividing the density profile everywhere by a factor of 4. The preheat deduced from the HXR detector is seen to be weakly dependent on the density (or the areal density) of the fuel. Thus,

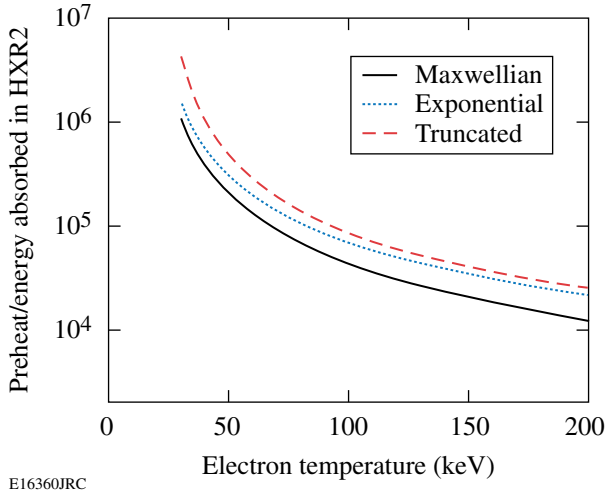

Figure 112.16
Ratio of energy deposited in D_2 by fast electrons to energy absorbed in HXR2 for three different distributions of fast-electron energies. Much of the variation between the three curves disappears when converting the absorbed x-ray energy to a detector signal (Fig. 112.17).

the validity of the preheat curves for CH (Fig. 112.14) and D_2 (Fig. 112.16) is quite general with a precision of ~25%. The uncertainty in the experimentally determined temperature adds an additional uncertainty. The curves for D_2 apply equally to a DT fuel since the loss rate dE/dx due to either collisions or radiation is independent of the atomic mass. The NIST tables are actually given in terms of $(1/\rho)$dE/dx; this is inconsequential for Mo or CH since only the ratio of the two losses is used. However, for the cryogenic targets, we use the NIST tables only for the collision rate; thus, the tables (which are for hydrogen) had to be restated in terms of dE/dx, for which case they are the same for either D_2 or DT.

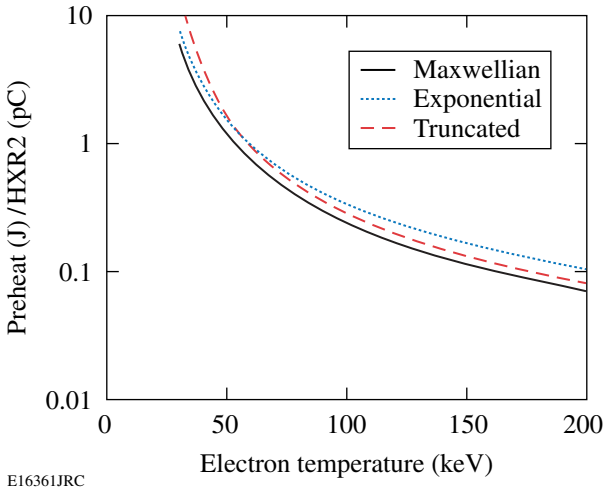

Figure 112.17
Ratio of energy deposited by fast electrons in D_2 to HXR2 reading (in pC) for three different distributions of fast-electron energies. The preheat deduced from the HXR detector is seen to be weakly dependent on the assumed electron distribution.

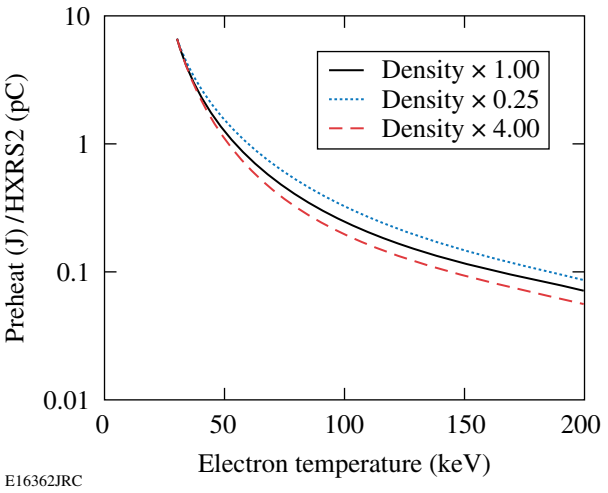

Figure 112.18
Ratio of energy deposited by fast electrons in D_2 to HXR2 reading (in pC) for a Maxwellian distribution of fast-electron energies and three different multipliers of the *LILAC*-simulated density profile. The preheat deduced from the HXR detector is seen to be weakly dependent on the density (or the areal density) of the fuel.

The *LILAC*-calculated density profile shows a sharp, well-defined cold shell of ~4-g/cm^3 density. Since the preheating of this cold shell is particularly relevant to target-performance degradation, we calculated the fraction of energy deposited within this shell, assuming the electrons move radially. For all temperatures above ~50 keV, this fraction is about constant at ~0.8 and drops at lower temperatures. This is an upper limit on the fraction of energy deposited in the cold shell, as 2-D effects will lower it. It should be noted that the HXR signal in the ordinates of Figs. 112.16 and 112.17 apply only to the x-ray emission from the fuel, not the CH. Thus, before applying these figures to a particular cryogenic experiment, the fraction of the measured x-ray signal emitted by the fuel has to be determined by a code allowing for the 2-D trajectories of the electrons. No such complication arises in the case of CH-only targets. For these targets, the measured HXR signal yields the total energy absorbed as preheat in the target (integrated over time and space), with no need for 2-D calculation of the electron trajectories. This is also shown in Fig. 112.15 by the independence of the ratio x ray/preheat on the target thickness.

An important result derived from these calculations relates to the determination of the temperature from the measured signals in three of the four HXR channels. The shape of the bremsstrahlung spectrum in these determinations[2] is customarily assumed to be exponential [~exp(–E/T)]. However, calculating the x-ray spectrum for a variety of assumed electron-energy distributions shows that the x-ray spectrum deviates from an exponential. Figure 112.19 shows the calculated bremsstrahlung spectrum for three different electron-distribution functions plotted versus photon energy normalized to the fast-electron temperature. They are obtained by averaging the spectrum from a single-electron energy[1] over the electron-energy distribution. We see that even for an assumed exponential distribution for the electrons, the distribution for the photons is not exponential, except for high E/T. The curve marked "slope" represents the exponential spectrum assumed in the derivation of the temperature from the HXR signals. Therefore, the HXR data have to be fitted with one of the curves shown in Fig. 112.19. The HXR channels are dominated by radiation in the range ~50 to 80 keV determined by the channel filters. Thus, for temperatures higher than ~80 keV, relevant values of E/T are smaller than 1 and the

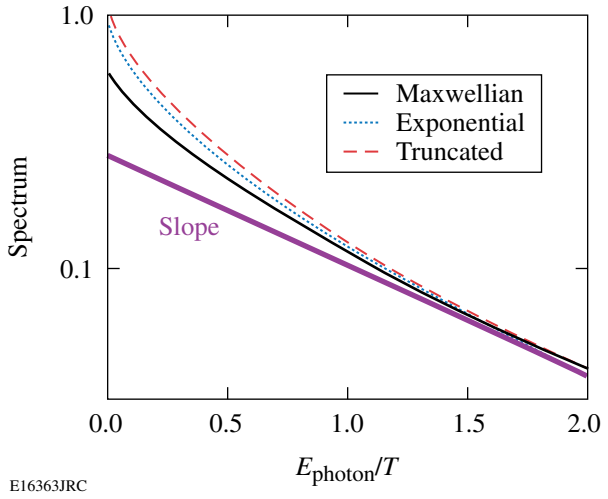

Figure 112.19
Bremsstrahlung spectrum calculated using tabulated values from Seltzer and Berger,[4] on which NIST slowing-down tables are based. The spectra for each electron energy were averaged over three different electron-distribution functions and plotted versus photon energy normalized to the fast-electron temperature.

derived temperature would be lower than the true temperature (given by the curve marked "slope"). The correction increases with temperature. For a measured value of T = 100 keV, the correct temperature is estimated to be ~130 keV. The corrected temperature would reduce the determined preheat for a given measured HXR signal. Using Fig. 112.17 we estimate that the derived preheat for fast-electron temperatures in the range of 100 to 200 keV would drop by ~50%. This indicates that even for high values of laser irradiance, the preheat by fast electrons may not be an important factor in explaining the degradation in compression.

In summary, an improved procedure for calculating preheat from the measured hard x-ray signal is described. The numerically calculated bremsstrahlung spectrum as a function of electron energy (E) is averaged over an assumed electron-energy distribution and folded with the HXR detector sensitivity. This is done for each value of E and each target location within a multi-group, 1-D electron-transport code. The results relate the measured HXR signal and fast-electron temperature to the preheat. A 2-D transport code has to be used to determine the fraction of the measured x-ray signal coming from the fuel for cryogenic experiments because of the two-material target composition. Additionally, the shape of the measured x-ray spectrum has been calculated; this shape has to be used in the fitting of the HXR channels data. This correct procedure will yield a higher fast-electron temperature than when assuming an exponential x-ray spectrum and, therefore, a lower preheat for a given HXR signal.

ACKNOWLEDGMENT

This work was supported by the U.S. Department of Energy Office of Inertial Confinement Fusion under Cooperative Agreement No. DE-FC52-92SF19460, the University of Rochester, and the New York State Energy Research and Development Authority. The support of DOE does not constitute an endorsement by DOE of the views expressed in this article.

REFERENCES

1. B. Yaakobi, C. Stoeckl, W. Seka, J. A. Delettrez, T. C. Sangster, and D. D. Meyerhofer, Phys. Plasmas **12**, 062703 (2005).

2. C. Stoeckl, V. Yu. Glebov, D. D. Meyerhofer, W. Seka, B. Yaakobi, R. P. J. Town, and J. D. Zuegel, Rev. Sci. Instrum. **72**, 1197 (2001).

3. M. J. Berger, J. S. Coursey, and M. A. Zucker, *ESTAR*, *PSTAR*, and *ASTAR*: Computer Programs for Calculating Stopping-Power and Range Tables for Electrons, Protons, and Helium Ions (version 1.2.2). [Online] Available: http://physics.nist.gov/Star [25 February 2005]. National Institute of Standards and Technology, Gaithersburg, MD.

4. S. M. Seltzer and M. J. Berger, Nucl. Instrum. Methods Phys. Res. B **12**, 95 (1985).

5. R. H. Pratt *et al*., At. Data Nucl. Data Tables **20**, 175 (1977).

6. J. D. Jackson, *Classical Electrodynamics*, 2nd ed. (Wiley, New York, 1975).

7. C. J. Powell, Rev. Mod. Phys. **48**, 33 (1976).